

Is Independence all you need? On the Generalization of Representations Learned from Correlated Data

Frederik Träuble

MPI for Intelligent Systems

FREDERIK.TRAEUBLE@TUEBINGEN.MPG.DE

Elliot Creager

University of Toronto and Vector Institute

Niki Kilbertus

MPI for Intelligent Systems and University of Cambridge

Anirudh Goyal

Mila and Université de Montréal

Francesco Locatello

ETH Zurich and MPI for Intelligent Systems

Bernhard Schölkopf

MPI for Intelligent Systems

Stefan Bauer

MPI for Intelligent Systems

Abstract

Despite impressive progress in the last decade, it still remains an open challenge to build models that generalize well across multiple tasks and datasets. One path to achieve this is to learn meaningful and compact representations, in which different semantic aspects of data are structurally disentangled. The focus of disentanglement approaches has been on separating independent factors of variation despite the fact that real-world observations are often not structured into meaningful independent causal variables to begin with. In this work we bridge the gap to real-world scenarios by analyzing the behavior of most prominent methods and disentanglement scores on correlated data in a large scale empirical study (including 3900 models). We show that systematically induced correlations in the dataset are being learned and reflected in the latent representations, while widely used disentanglement scores fall short of capturing these latent correlations. Finally, we demonstrate how to disentangle these latent correlations using weak supervision, even if we constrain this supervision to be causally plausible. Our results thus support the argument to learn independent mechanisms rather than independent factors of variations.

1. Introduction

A complex generative model can be thought of as the composition of independent mechanisms or “causal” modules, which generate high-dimensional observations (such as images or videos). In the causality community, this is often considered a prerequisite to achieve representations which are robust to interventions upon variables determined by such models (Peters et al., 2017; Suter et al., 2019; Goyal et al., 2019). One particular instantiation of this idea in the machine learning community is the notion of *disentangled* representations (Bengio et al.,

2013). The goal of disentanglement learning is to find a representation of the data which captures all the ground-truth factors of variation (FoV) independently.

Due to the induced structure, disentangled representations promise generalization to unseen scenarios (Higgins et al., 2017b), increased interpretability (Adel et al., 2018; Higgins et al., 2018) and faster learning on downstream tasks (van Steenkiste et al., 2019; Locatello et al., 2019a). While the advantages of disentangled representations have by now been well established, they generally assume independence in the latent space, which is rarely the case for higher-level factors of variation in real world settings. As an example, consider a scene with a table and some chairs (see Figure 1). The higher-level factors of this representation are in fact correlated and what we actually want to infer are independent (causal) mechanisms (Peters et al., 2017; Suter et al., 2019; Goyal et al., 2019; Parascandolo et al., 2018).

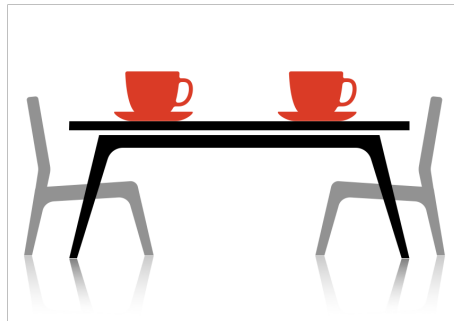


Figure 1: Common observational scenario displaying co-occurring independent causal mechanisms (coffee cup, table, chair) which manifest as data correlations since the objects typically appear together.

Despite the recent growth of the field, the performance of state-of-the-art disentanglement learning in more correlated realistic settings is unknown. Given the potential societal impact in the medical domain (Chartsias et al., 2018) or fair decision making (Locatello et al., 2019a; Madras et al., 2018; Creager et al., 2019), the evaluation of the usefulness of disentangled representations trained on correlated data is of critical importance.

To bridge the gap between the idealistic settings considered thus far and the real world, we conducted a large scale empirical study to systematically study the effect of artificially introduced correlations between pairs of factors of variation in training data on the learned representations. To provide a qualitative and quantitative evaluation, we investigate multiple datasets where we have still access to ground-truth labels. Moreover, we study the generalization abilities of the representations learned on correlated data as well as their performance in particular for the downstream task of fair decision making.

Contributions. Our main contributions can be summarized as follows:

- We present the first large-scale empirical study (3900 models)¹ that examines how modern disentanglement learners cope with *correlated* observational data;
- We find that factorization-based inductive biases are insufficient to learn disentangled representations from observational data. Existing methods fail to disentangle correlated factors of variation, and moreover standard disentanglement metrics are insufficient to reveal these troublesome pairwise entanglements.

1. Each model is trained for 300,000 iterations on Tesla V100 GPUs. Reproducing these experiments requires approximately 0.72 GPU years

- We examine how the model encodes data where the train-time correlation is broken (OOD w.r.t. train set). The factorized prior induces strong latent structure that helps the model generalize, suggesting that the latent pair-wise correlations could be corrected.
- We present two approaches to resolving correlation entanglement in the latent code when some knowledge of the dataset bias/correlation is available. We focus in particular on the use of weak labels that are *causally plausible*, underscoring the promise of causal inductive biases in resolving shortcoming in current disentanglement methods highlighted by our empirical study.

2. Background and Related Work

Disentanglement. Current state-of-the-art disentanglement approaches use the framework of variational auto-encoders (VAEs) (Kingma and Welling, 2014). The (high-dimensional) observations \mathbf{x} are modelled as being generated from some latent features \mathbf{z} with chosen prior $p(\mathbf{z})$ according to the probabilistic model $p_\theta(\mathbf{x}|\mathbf{z})p(\mathbf{z})$. The generative model $p_\theta(\mathbf{x}|\mathbf{z})$ as well as the proxy posterior $q_\phi(\mathbf{z}|\mathbf{x})$ can be represented by neural networks, which are optimized by maximizing the variational lower bound (ELBO) of $\log p(\mathbf{x}_1, \dots, \mathbf{x}_N)$.

$$\mathcal{L}_{VAE} = \sum_{i=1}^N \mathbb{E}_{q_\phi(\mathbf{z}|\mathbf{x}^{(i)})} [\log p_\theta(\mathbf{x}^{(i)}|\mathbf{z})] - D_{KL}(q_\phi(\mathbf{z}|\mathbf{x}^{(i)})||p(\mathbf{z})) \quad (1)$$

Since the above objective does not enforce any structure on the latent space, except for some similarity to the typically chosen isotropic Gaussian prior $p(\mathbf{z})$, various proposals for more structure imposing regularization have been made. In this work we consider the standard protocol in `disentanglement_lib` from Locatello et al. (2019b) covering six state-of-the-art VAE regularizers for disentanglement and commonly used evaluation metrics measuring different notions of disentanglement of the learned representations (Higgins et al., 2017a; Kim and Mnih, 2018; Burgess et al., 2018; Kumar et al., 2018; Chen et al., 2018; Eastwood and Williams, 2018; Locatello et al., 2019a). More details about the methods we use can be found in the Appendix. Recently, it has been shown that purely unsupervised learning of disentangled representations is impossible (Locatello et al., 2019b, Theorem 1). To address this theoretical limitation, methods have been proposed that do not require explicitly labelled data but only some weak labeling information (Locatello et al., 2020; Shu et al., 2019). We will address one of these methods in more detail in Section 4.

Correlations. Whenever a joint distribution of random variables does not satisfy the mathematical property of probabilistic independence, then there has to be a dependence between its random variables, often referred to as correlation.² Specifically, the dependence holds for a set of random variables $X_{i=1, \dots, n}$ if and only if

$$P(X_1, X_2, \dots, X_n) \neq \prod_{i=1}^n P(X_i). \quad (2)$$

Although a dependence or correlation between two variables can indicate a causal relationship, correlation can also be due to unobserved confounders and it does thus not imply a direct

2. We use the term correlation here in a broad sense of any statistical association, not just linear dependencies.

causal link. Real-world datasets display many of these (“spurious” and often a priori unknown) correlations Geirhos et al. (2020). The disentanglement community, on the other hand, often assumes that there is an underlying set of independent ground truth variables in the generative process of observations. These methods are hence predominantly evaluated on data that obeys independence in the true factors of variation, which we deem the right factorization. In the real world, the observation generating process is likely not always as clearly “disentangled” and we do expect correlations in the collected datasets. It is thus an open question to what degree existing inductive biases from the encoder/decoder architecture, but more importantly the dataset biases, affect the learned representation. In our experiments, we introduce (simple) dataset correlations in a controlled manner to understand to what degree state-of-the-art approaches can cope with such correlations. We believe these correlations to reflect a major feature of more realistic environments.

Other Related Work Most popular datasets in the disentanglement literature exhibit perfect independence in their FoV. At some level this is sensible as it reflects the underlying assumption in the inductive bias being studied. However, this assumption is unlikely to hold in practice. The literature so far has not thoroughly measured how popular inductive biases such as factorized priors behave when learning from correlated datasets, although several smaller experiments along these lines can be acknowledged. Chen et al. (2018) studied correlated 3DFaces (Paysan et al., 2009) by fixing all except three factors in which the authors conclude that the β -TC-VAE regularizer can help to disentangle imposed correlations. However, the latent structure was not studied in detail; our findings suggest that global disentanglement metrics are insufficient to diagnose issues when models learn from correlated data. Creager et al. (2019) based some of the evaluations of a proposed new autoencoder architecture in the fairness context on a biased dSprites variant. However, their study focused on representation learners that require strong supervision via FoV labels at train time (inference does not require labels).

3. The effect of correlated data on disentanglement learners

3.1 Experimental design

For our first experiments we introduce correlations between single pairs of factors of variation on the following three datasets: Shapes3D with object size and azimuth (denoted “A”), dSprites with orientation and X-position (“B”) and finally the real-world observations dataset MPI-3D with first and second degree of freedom (“C”). For simplicity, we focused on a linear correlation with Gaussian noise between both variables parametrized by $P(z_{c1}, z_{c2}) \sim \mathcal{N}(z_{c2} - \alpha z_{c1}, \sigma)$ where $\alpha = z_{c2}^{max} / z_{c1}^{max}$ with labels of the FoV starting from 0. The strength of the correlations is being tuned with three different line widths σ : 0.2, 0.4, 0.7 in normalized units with respect to the range of values in $z_{c1, c2}$. Thus, lower σ indicates a stronger correlation. Additionally, we study the uncorrelated limit ($\sigma = \infty$), a control case that matches the conditions typically studied in the literature. In the Appendix we show the corresponding joint distributions. We train the same six VAE methods as discussed in (Locatello et al., 2019b), including β -VAE, FactorVAE, AnnealedVAE, DIP-VAE-I, DIP-VAE-II and β -TC-VAE, each with six hyperparameter settings. Each method has been trained using five different random seeds.

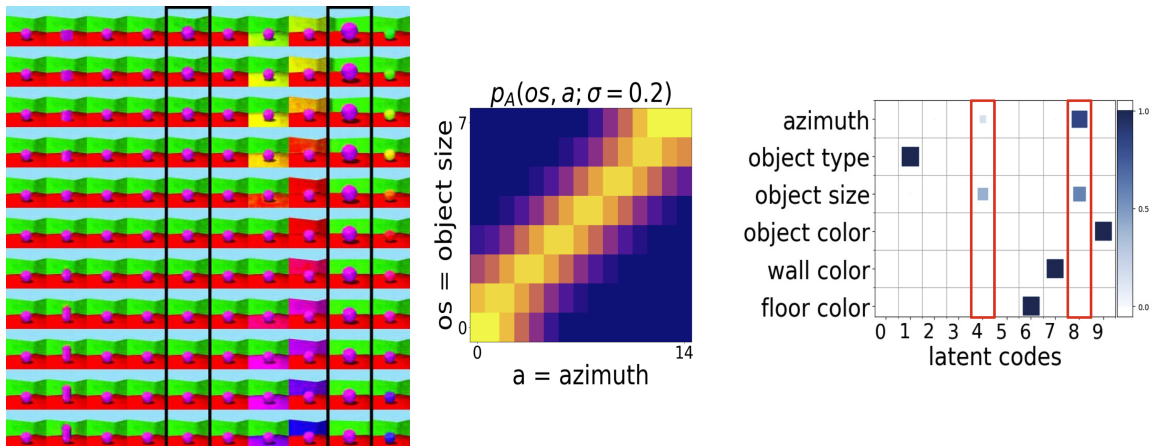


Figure 2: We show latent traversals (left) of the best DCI score model among all 180 trained models with strongest correlation ($\sigma = 0.2$) on Shapes3D (A). The traversals in latent code dimensions 4 and 8 (highlighted in black), suggest that these dimensions encode a mixture of azimuth and object size, reflecting one major axis along the correlation line of the joint distribution (middle) and one smaller, locally orthogonal axis. This is supported by the GBT feature importance matrix of this model (right) indicating an entanglement of azimuth and object size encoded into both latent codes. Additional entanglement analysis can be seen in Figure 11 in the Appendix.

All remaining factors of variation are sampled uniformly at random. This first study sums up to a total of 2160 trained models, or 180 models per dataset and correlation strength.

3.2 Can unsupervised methods achieve disentanglement of correlated data?

Shortcomings of existing metrics Following recent studies, we evaluate the trained models with the help of a broad range of disentanglement metrics that aim at quantifying overall success by the help of a single scalar measure. Perhaps surprisingly, we see no clear trend between all covered disentanglement scores w.r.t. correlation strength. The metrics have been evaluated by sampling from the correlated data distribution although they do not differ substantially when evaluated on the uncorrelated distribution. See Figure 9 and 10 in the Appendix which show this finding across all methods and metrics. We thus argue that commonly used methods are insufficient to provide insight into the latent space learned. As we will see below, the latent spaces show some characteristic differences when trained on a strongly correlated pair of FoVs. To conduct a more careful analysis of the inductive data bias applied on the learned representations we instead utilize pairwise metrics.

Latent structure and pairwise disentanglement. We start by analysing latent traversals of some trained models on Shapes3D. For strong correlations ($\sigma = 0.2$ and $\sigma = 0.4$), we typically observe trained models with two latent codes encoding the two correlated variables simultaneously. In these cases, one of the latent codes corresponds to data along the major axis of the correlation line whereas the other latent code dimension manifests in an orthogonal change of the two variables along the minor axis. Still, a full traversal of the code

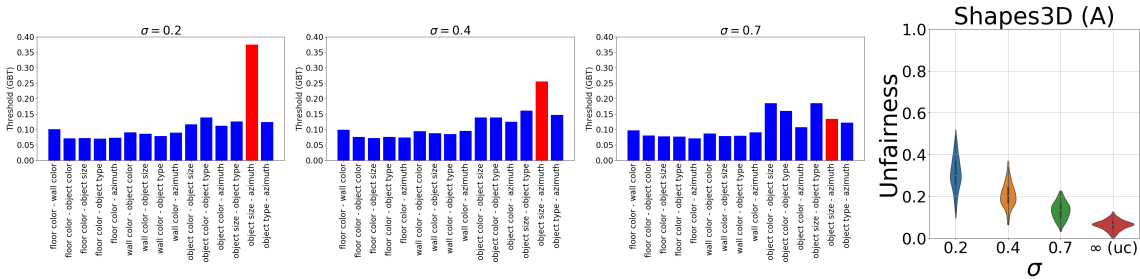


Figure 3: Pairwise disentanglement scores help to uncover still existent correlations in the latent representation. Left: Mean of the pairwise entanglement scores across all 180 models in Shapes3D (A), showing that stronger correlation leads to more entanglement. The correlated pair of factors is highlighted (red). The same behavior can be seen for the unfairness score between the correlated pair of factors (right).

corresponding to the minor axis often seems to cover only observations within the correlation line. Figure 2 shows this effect for the latent space of the model trained on Shapes3D and strongest correlation (0.2) with the highest DCI score (common disentanglement metric).

To quantify this observation, we analyze the importance of individual latent codes in predicting the value of a given ground truth FoV. These weights are inferred by training a gradient boosting trees (GBT) classifier between the latents and their ground truth labels (10,000 samples). For this particular model, results are shown in Figure 2. The corresponding evaluation for a model trained on the same dataset with weak correlation does not reveal this feature (see Figure 12 in the Appendix).

To support this claim beyond some selected models, we first evaluate a recently introduced pairwise disentanglement score (Locatello et al., 2019b) across all FoV pairs and report the respective mean across all models. This score is based on a threshold metric inferred from a bidirectional graph between latents and FoVs based on the GBT feature importance matrix. In Figure 3 (left) we show these scores on the correlated Shapes3D dataset. Interestingly, the pair of correlated FoV is the most difficult one to disentangle across the large parameter sweep of models. This threshold decreases with weaker correlation and the pair becomes easier to disentangle than other non-correlated pairs for weaker correlations ($\sigma \geq 0.7$). The same trends for the other datasets are shown in Figure 13 in the Appendix. These findings suggest that the models can disentangle correlated factors if the correlation is not too strong, e.g. as supported for a specific model in Figure 12. Similar conclusions can be drawn when basing the calculation of this metric on the mutual information instead, which we show in the Appendix in Figure 14, 15 and 16. In line with these results, we observe a weak trend towards a higher predictability score of all FoVs on models with stronger correlation as can be seen in the Appendix in Figure 17.

Finally, we investigate some fairness ramifications of these entangled latent spaces by computing another pairwise metric: An unfairness score of predicting the second correlated variable while the first correlated variable is considered being a protected or sensitive attribute. For this we use a variant of demographic parity Dwork et al. (2012) that computes pairwise

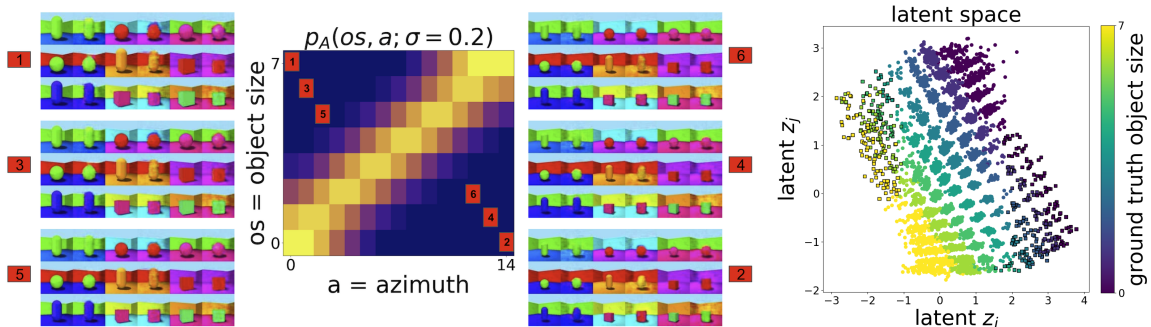


Figure 4: Generalization to out-of-distribution (OOD) test data. Left: Reconstructions of observations the model has never seen during training. Right: Latent space distribution of the two entangled dimensions. Circles without edges indicates encoded data from the (correlated) training distribution, while circles with edges indicate encoded OOD data where the correlation pattern is broken.

mutual information between latents and FoV (Locatello et al., 2019a). In Figure 3 (right) we evaluate this score when correlations are present within the data. Unfairness tracks correlation strength in this scenario. The same trend can be seen for the other correlated datasets (Figure 18). These results suggest that we cannot expect disentangled representations learned unsupervisedly to help reduce unfairness beyond the benefits discussed in Locatello et al. (2019a).

3.3 Generalization Properties

In this Section, we aim to understand how the trained models perform on unseen training data far away from the correlation line (OOD w.r.t. the train distribution). We analyse this capability for the model from Figure 2. In this model, the remaining factors seem to be disentangled well enough to only focus on the two latent dimensions encoding the entangled variables.

As a first test, we sample observations from the FoV then set object size and azimuth to six distinct configurations of zero probability (Figure 4). The trained model is capable of reconstructing these observations despite never having encountered these configurations or neighbors thereof during training. This suggests that the encoder maps representations to a meaningful point in the latent space from which the decoder is equally capable of generating expected observations. To test this hypothesis further, we analysed latent traversals originating from these OOD points (Figure 19). We observe that changes in the remaining factors reliably yield the expected reconstructions. Traversals with respect to the two entangled latent codes continue to encode object size and azimuth.

To fully understand this models' generalization properties we visualise the occupied latent space spanned by the two identified dimensions encoding both correlated factors in Figure 4. We are particularly interested in where these points are located with respect to the ground truth value of each correlated variable, depicted via color. The two sets of depicted points are

(1) latent codes sampled from the correlated training data and (2) latent codes sampled with a (object size, azimuth) configuration that has zero probability under the correlated training distribution. We observe that contours of equal color (ground truth) are not aligned with the plot axes. This indicates that the two latent dimensions encode both FoV at the same time. Likewise, we can understand the generalization capabilities of this model far away from the trained data. Extreme configurations such as (small azimuth, large object size) are encoded to space regions corresponding to the intersections of the manifolds with constant value for each correlated variable. This shows that all out-of-distribution points are encoded in this representation space in a way that obeys the natural ordering of each respective factor. This behaviour remains even in cases where the trained latent space does not mirror the default value ordering as stored in our ground truth table. For this we additionally trained two times 360 models on two additional Shapes3D variants where we strongly correlated object color - object size (“D”) and object color - azimuth (“E”) respectively ($\sigma = 0.2$ and $\sigma = 0.4$). As the color values do not allow for a unique natural ordering, the trained models do often encode a different color manifold ordering into the latent space. Figure 20 in the Appendix shows some characteristic latent space visualizations with similar extrapolation and generalization capabilities. We conclude from these results that disentanglement methods can generalize towards unseen FoV configurations as long as each factor value is contained in the training data within a different configuration.

4. Finding the right factorization

The results from Section 3 illustrate the limitations of state-of-the-art unsupervised methods on correlated data (and thus real-world observational data). We now propose several approaches to mitigating pairwise correlations in the latent code. We begin with a post-hoc procedure that uses limited label information on the ground truth factors, then consider an approach leveraging recent advances in weakly supervised disentanglement learning that applies directly at train time.

4.1 Post-hoc alignment correction with few labels

When limited FoV labels for the correlated train set can be accessed, we suggest to resolve entangled dimensions of the latent code by *fast adaptation*. To identify the two entangled dimensions (z_i, z_j) we look at the maximum GBT feature importance for a given FoV. We then train a *substitution function* using supervised learning to replace these two dimensions with the predicted ground truth label. Crucially, both steps of this procedure should rely on as few FoV labels as possible. In Figures 5 and 21 we implement fast adaptation with a linear regression as the substitution function, which succeeds with as few as 100 labels, corresponding to less than 0.02% of all data points in Shapes3D. This method improves the pairwise-disentanglement across the ensemble of all trained models in Shapes3D with correlated object size and azimuth (Figure 22). However, fast adaptation with linear regression substitution fails in some settings: when no two latent dimensions encode the applied correlation isolated from the other latent codes, or when the correlated variables do not have a unique natural ordering (e.g. color or categorical variables). Additionally, the functional form of the latent manifolds beyond the training distribution is unknown and in general expected to be nonlinear. We test the possibility of fast adaptation in this case

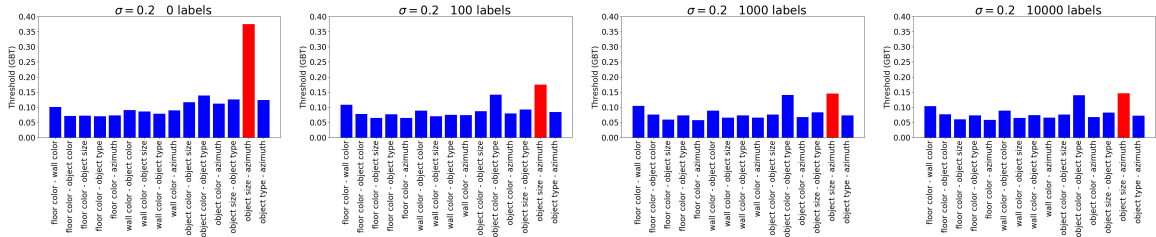


Figure 5: Pairwise disentanglement scores for all pairs of variables in Shapes3D. The correlated pair is highlighted (red). Left plot is the unsupervised baseline without any fast adaptation. Other plots show that fast adaption using linear regression reduces these correlations with as little as 100 labels.

using as substitution function a one-hidden layer MLP classifier of size 100 on the correlated Shapes3D variants. Under this method, we sample the FoV from a uniform independent distribution. A small number of such samples could practically be labeled manually. Using only 1000 labeled data points for our fast adaptation method shows a significant reduction in disentanglement-thresholds for the correlated pair (Figure 23).

We find that the efficacy of fast adaptation depends on the level of disentanglement of the representations with respect to all the other factors. This implies that if the representation is well disentangled at the start of the fast adaption procedure, it is possible to achieve a perfectly disentangled model (according to our previous visual and quantitative evaluations). However, if all FoV are entangled at the beginning, the fast adaption method will have little effect. Finally, we note that model selection is impossible in a purely unsupervised manner based on any of the used disentanglement metrics, as they all require labeled ground truth data. These shortcomings shall be resolved by the following method capable of disentangling the correlated factors of variation much more reliably.

4.2 Alignment during training using weak supervision

Since the purely unsupervised learning of disentangled representations is impossible (Locatello et al., 2019b, Theorem 1), inductive biases like grouping information (Bouchacourt et al., 2018) or access to labels (Locatello et al., 2019c) is required. Changes in natural environments, which typically correspond to changes of only a few underlying factors of variation, provide a weak supervision signal for representation learning algorithms (Goyal et al., 2019; Földiák, 1991; Schmidt et al., 2007; Bengio et al., 2019). Without correlations it has been shown that this weak supervision helps in learning much more disentangled representations in (Locatello et al., 2020; Shu et al., 2019). Locatello et al. (2020) showed access to observations which display differences in a known number of factors of variation (without knowing which ones specifically) is sufficient to learn disentangled representation. These additional weak assumptions render the generative model identifiable in contrast to unsupervised disentanglement. This kind of extra knowledge is often available at no cost³, e.g., in temporarily close frames from a

3. On the other hand, in applications with fairness concerns it may be impossible to intervene on FoV representing sensitive and immutable attributes of individuals (gender, race, etc.); we refer to Madras et al. (2019) for a more complete discussion.

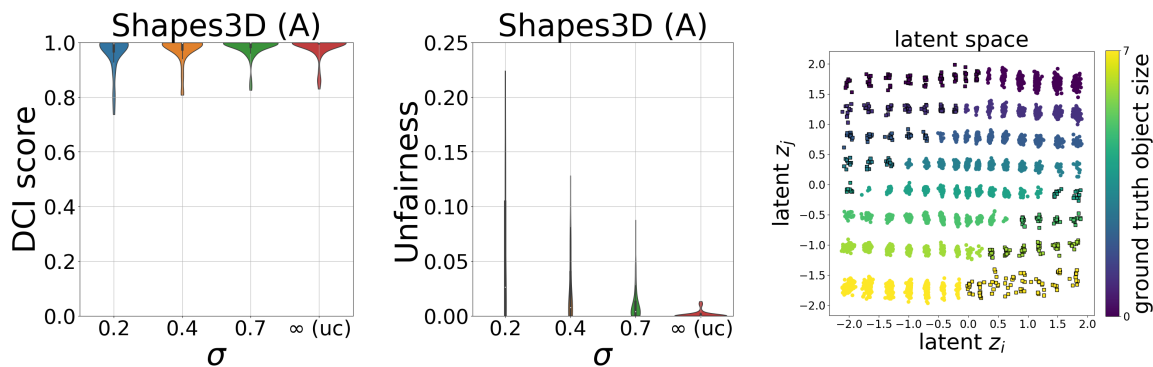


Figure 6: Left: With weak supervision trained models on Shapes3D correlation object size and azimuth learn consistently improved, often perfect, disentangled representation across all correlation strengths. Middle: Unfairness scores between correlated FoVs are much smaller (see scale). Right: Latent dimensions of a best DCI model with strong correlation (0.2). Representations are perfectly axis-aligned with respect to both of the correlated variables ground truth values (right).

video of a moving robot arm where some factors remain unchanged. Formally, this implies for the true posterior of a pair of observations $p(z_i|\mathbf{x}_1) = p(z_i|\mathbf{x}_2)$ for shared factors and $p(z_i|\mathbf{x}_1) \neq p(z_i|\mathbf{x}_2)$ for changing factors. To enforce these structural constraints into the latent space, the constant dimensions are estimated from the smallest dimension-wise KL divergences. We use the same min-max threshold as applied in the original method. For dimensions with constant factors of variation we then replace the posterior by an average of the two observations and optimize the pairwise observation variant of the β -VAE objective from the original paper. Besides this, the method allows for model selection via the (unsupervised) reconstruction loss (Locatello et al., 2020).

Weakly supervision mitigates pairwise latent entanglement We trained the three previously introduced Shapes3D variants (A, D, E) with pairwise correlations between object color, object size and azimuth with the same correlation strength settings. Due to the definition of the regularizer we limit this study to the β -VAE models with the same 6 hyperparameters but use 10 random seeds instead, yielding 720 additional models. For the sampling of pairs we study the case where a change in one random FoV is induced, keeping all others constant. In a first study we do not make any additional assumptions about the origin of the correlations and assume that we can break the correlation whenever we sample the change to be in one of the correlations. The value of the changing variable is sampled uniformly in the second observation. This might be applicable to situations where the generator of the pairs of observations is not fully aware of the correlations or has intervention capabilities on all correlated variables.

Figure 6 summarizes the weak supervision results when imposing correlations in object size and azimuth. We consistently observe much better disentangled models, often achieving perfect DCI score irrespective of correlations in the dataset. Moreover, the latent spaces tend to strongly align their coordinates with the ground truth label axis. Finally, weak

supervision reduces unfairness relative to the unsupervised baseline, and occasionally achieves zero unfairness score. Respective results showing the same strong improvements for the other correlated Shapes3D datasets can be seen in Figures 24 –31 in the Appendix. These results suggest that weak supervision can provide a strong inductive bias capable of finding the right factorization and resolving spurious correlations for datasets of unknown degree of correlation. As a prominent example, this is an issue in the fairness context where real-world datasets often display unknown discriminatory correlations.

Causally plausible weak supervision As discussed above, correlation does not imply causation since a multiplicity of causal generative models can yield the same correlation structure. Because the proposed method starts with the premise that weak supervision is available at train time, it is also important to validate that the method provides a benefit when the supervision is *causally plausible*, i.e. reflects the true causal process generating the correlated distribution (rather than some erroneous one). In the causal view, we can interpret the fixing of all but one factor as an intervention (Pearl, 2009). Changes in the sampled factor are restricted by the causal graph. Let us assume C_1 causes C_2 in our examples, which manifests as the studied linear correlations. Within this setting we cannot sample uniformly in C_2 if we intervene on all factors except for this causal factor. Intervening on all factor but C_1 , however, allows us to sample all values for this factors as it is not causally affected by C_2 . To test the hypothesis that this constraint still allows for disentangling the correlation, we trained on the Shapes3D (A) and sample pairs consistent with the causal generative model only. Besides observing visually disentangled factors in the latent traversals, we show in Figure 7 the same significant improvement in DCI score with respect to the unsupervised case. Similar results can be seen in all the other disentanglement metrics in the Appendix in Figure 32. Besides the above correlation strengths, we additionally trained the same models using a very strong correlation of $\sigma = 0.1$, yielding 300 models trained in this study. Additionally, we support the claim of disentangled correlations by showing the latent space of the lowest reconstruction loss model trained under a correlation $\sigma = 0.1$ in Figure 33 in the Appendix.

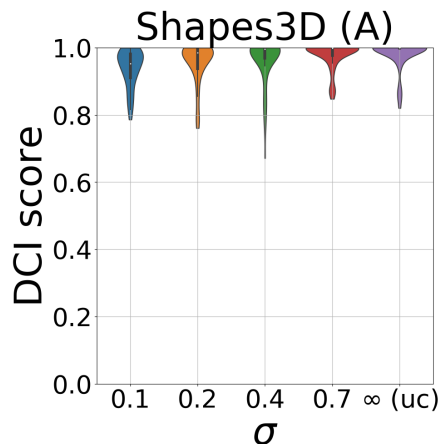


Figure 7: Correlations can be disentangled using weak supervision if the pair sampling follows a causal generative model.

5. Conclusion

We have presented the first large-scale empirical study that examines how modern disentanglement learners cope with correlated observational data. We find that existing methods fail to learn disentangled representations of correlated factors of variation, and moreover that standard disentanglement metrics are insufficient to reveal these troublesome pairwise entanglements. We discussed practical implications for downstream tasks like fair decision

making and generally observe that we can correct for these latent correlations even if possible interventions are restricted to the underlying causal graph. Our results thus support the argument to learn independent mechanisms rather than independent factors of variations. Besides the simple correlations studied in this work, future work is needed to address the open question whether these results extend to more complex nonlinear correlations and settings where many more variables are correlated simultaneously.

References

- Tameem Adel, Zoubin Ghahramani, and Adrian Weller. Discovering interpretable representations for both deep generative and discriminative models. In *International Conference on Machine Learning*, pages 50–59, 2018.
- Yoshua Bengio, Aaron Courville, and Pascal Vincent. Representation learning: A review and new perspectives. *IEEE Transactions on Pattern Analysis and Machine Intelligence*, 35(8):1798–1828, 2013.
- Yoshua Bengio, Tristan Deleu, Nasim Rahaman, Rosemary Ke, Sébastien Lachapelle, Olexa Bilaniuk, Anirudh Goyal, and Christopher Pal. A meta-transfer objective for learning to disentangle causal mechanisms. *arXiv preprint arXiv:1901.10912*, 2019.
- Diane Bouchacourt, Ryota Tomioka, and Sebastian Nowozin. Multi-level variational autoencoder: Learning disentangled representations from grouped observations. In *AAAI Conference on Artificial Intelligence*, 2018.
- Christopher P Burgess, Irina Higgins, Arka Pal, Loic Matthey, Nick Watters, Guillaume Desjardins, and Alexander Lerchner. Understanding disentangling in beta-VAE. *arXiv preprint arXiv:1804.03599*, 2018.
- Agisilaos Chatsias, Thomas Joyce, Giorgos Papanastasiou, Scott Semple, Michelle Williams, David Newby, Rohan Dharmakumar, and Sotirios A Tsaftaris. Factorised spatial representation learning: Application in semi-supervised myocardial segmentation. In *International Conference on Medical Image Computing and Computer-Assisted Intervention*, pages 490–498. Springer, 2018.
- Tian Qi Chen, Xuechen Li, Roger Grosse, and David Duvenaud. Isolating sources of disentanglement in variational autoencoders. In *Advances in Neural Information Processing Systems*, 2018.
- Elliot Creager, David Madras, Jörn-Henrik Jacobsen, Marissa A Weis, Kevin Swersky, Toniann Pitassi, and Richard Zemel. Flexibly fair representation learning by disentanglement. *arXiv preprint arXiv:1906.02589*, 2019.
- Cynthia Dwork, Moritz Hardt, Toniann Pitassi, Omer Reingold, and Richard Zemel. Fairness through awareness. In *Proceedings of the 3rd innovations in theoretical computer science conference*, pages 214–226. ACM, 2012.

- Cian Eastwood and Christopher KI Williams. A framework for the quantitative evaluation of disentangled representations. In *International Conference on Learning Representations*, 2018.
- Peter Földiák. Learning invariance from transformation sequences. *Neural Computation*, 3(2):194–200, 1991.
- Robert Geirhos, Jörn-Henrik Jacobsen, Claudio Michaelis, Richard Zemel, Wieland Brendel, Matthias Bethge, and Felix A Wichmann. Shortcut learning in deep neural networks. *arXiv preprint arXiv:2004.07780*, 2020.
- Anirudh Goyal, Alex Lamb, Jordan Hoffmann, Shagun Sodhani, Sergey Levine, Yoshua Bengio, and Bernhard Schölkopf. Recurrent independent mechanisms. *arXiv preprint arXiv:1909.10893*, 2019.
- Irina Higgins, Loic Matthey, Arka Pal, Christopher Burgess, Xavier Glorot, Matthew Botvinick, Shakir Mohamed, and Alexander Lerchner. beta-VAE: Learning basic visual concepts with a constrained variational framework. In *International Conference on Learning Representations*, 2017a.
- Irina Higgins, Arka Pal, Andrei Rusu, Loic Matthey, Christopher Burgess, Alexander Pritzel, Matthew Botvinick, Charles Blundell, and Alexander Lerchner. Darla: Improving zero-shot transfer in reinforcement learning. In *International Conference on Machine Learning*, 2017b.
- Irina Higgins, Nicolas Sonnerat, Loic Matthey, Arka Pal, Christopher P Burgess, Matko Bošnjak, Murray Shanahan, Matthew Botvinick, Demis Hassabis, and Alexander Lerchner. Scan: Learning hierarchical compositional visual concepts. In *International Conference on Learning Representations*, 2018.
- Hyunjik Kim and Andriy Mnih. Disentangling by factorising. In *International Conference on Machine Learning*, 2018.
- Diederik P Kingma and Max Welling. Auto-encoding variational Bayes. In *International Conference on Learning Representations*, 2014.
- Abhishek Kumar, Prasanna Sattigeri, and Avinash Balakrishnan. Variational inference of disentangled latent concepts from unlabeled observations. In *International Conference on Learning Representations*, 2018.
- Francesco Locatello, Gabriele Abbati, Thomas Rainforth, Stefan Bauer, Bernhard Schölkopf, and Olivier Bachem. On the fairness of disentangled representations. In *Advances in Neural Information Processing Systems*, pages 14584–14597, 2019a.
- Francesco Locatello, Stefan Bauer, Mario Lucic, Sylvain Gelly, Bernhard Schölkopf, and Olivier Bachem. Challenging common assumptions in the unsupervised learning of disentangled representations. In *International Conference on Machine Learning*, 2019b.

- Francesco Locatello, Michael Tschannen, Stefan Bauer, Gunnar Rätsch, Bernhard Schölkopf, and Olivier Bachem. Disentangling factors of variation using few labels. *The 2nd Learning from Limited Labeled Data (LLD) Workshop at the International Conference on Learning Representations*, 2019c.
- Francesco Locatello, Ben Poole, Gunnar Rätsch, Bernhard Schölkopf, Olivier Bachem, and Michael Tschannen. Weakly-supervised disentanglement without compromises. *arXiv preprint arXiv:2002.02886*, 2020.
- David Madras, Elliot Creager, Toniann Pitassi, and Richard Zemel. Learning adversarially fair and transferable representations. *arXiv preprint arXiv:1802.06309*, 2018.
- David Madras, Elliot Creager, Toniann Pitassi, and Richard Zemel. Fairness through causal awareness: Learning causal latent-variable models for biased data. In *Proceedings of the Conference on Fairness, Accountability, and Transparency*, pages 349–358, 2019.
- G. Parascandolo, N. Kilbertus, M. Rojas-Carulla, and B. Schölkopf. Learning independent causal mechanisms. In *Proceedings of the 35th International Conference on Machine Learning (ICML)*, pages 4033–4041, 2018.
- Pascal Paysan, Reinhard Knothe, Brian Amberg, Sami Romdhani, and Thomas Vetter. A 3d face model for pose and illumination invariant face recognition. In *2009 Sixth IEEE International Conference on Advanced Video and Signal Based Surveillance*, pages 296–301. Ieee, 2009.
- Judea Pearl. *Causality*. Cambridge University Press, 2009.
- J. Peters, D. Janzing, and B. Schölkopf. *Elements of Causal Inference - Foundations and Learning Algorithms*. MIT Press, Cambridge, MA, USA, 2017.
- Mark Schmidt, Alexandru Niculescu-Mizil, Kevin Murphy, et al. Learning graphical model structure using l1-regularization paths. In *AAAI*, volume 7, pages 1278–1283, 2007.
- Rui Shu, Yining Chen, Abhishek Kumar, Stefano Ermon, and Ben Poole. Weakly supervised disentanglement with guarantees. *arXiv preprint arXiv:1910.09772*, 2019.
- Raphael Suter, Djordje Miladinović, Stefan Bauer, and Bernhard Schölkopf. Interventional robustness of deep latent variable models. In *International Conference on Machine Learning*, 2019.
- Sjoerd van Steenkiste, Francesco Locatello, Jürgen Schmidhuber, and Olivier Bachem. Are disentangled representations helpful for abstract visual reasoning? *arXiv preprint arXiv:1905.12506*, 2019.

Appendix A. Appendix

Unsupervised Disentanglement methods. For reasons of comparison, the considered disentanglement methods in this work cover the collection of studied state-of-the-art approaches in `disentanglement_lib` from Locatello et al. (2019b) based on representations learned by VAEs. The set contains six different methods that enforce disentanglement of the representation by equipping the loss with different regularizers that aim at enforcing the special structure of the posterior aggregate encoder distribution. A detailed description of the regularizer forms used in this work, specifically β -VAE (Higgins et al., 2017a), FactorVAE (Kim and Mnih, 2018), AnnealedVAE (Burgess et al., 2018), DIP-VAE-I, DIP-VAE-II (Kumar et al., 2018) and β -TC-VAE (Chen et al., 2018) is provided in (Locatello et al., 2019b). We use the same encoder architecture with 10 latent dimensions for every model.

Evaluation metrics. To measure disentanglement of a learned representation, various metrics have been proposed, each requiring access to the ground truth labels. The BetaVAE score is based upon the prediction of a fixed factor from the disentangled representation using a linear classifier (Higgins et al., 2017a). The FactorVAE score is intended to correct for some failures of the former by utilizing majority vote classifiers based on a normalized variance of each latent dimension (Kim and Mnih, 2018). The SAP score represents the mean distance between the classification errors of the two latent dimensions that are most predictable (Kumar et al., 2018). For the MIG score, one computes the mutual information between the latent representation and the ground truth factors and calculates the final score using a normalized gap between the two highest MI entries for each factor. Finally, the score proposed by Eastwood and Williams (2018), often referred to as DCI score, is calculated from a dimension-wise entropy reflecting the usefulness of the dimension to predict a single factor of variation.

An additional score of interest in this context is the fairness metric defined by Locatello et al. (2019a) which uses a notion of demographic parity for predicting a target variable y given a protected and sensitive variable s . Both y and s can be associated with a factor of variation here.

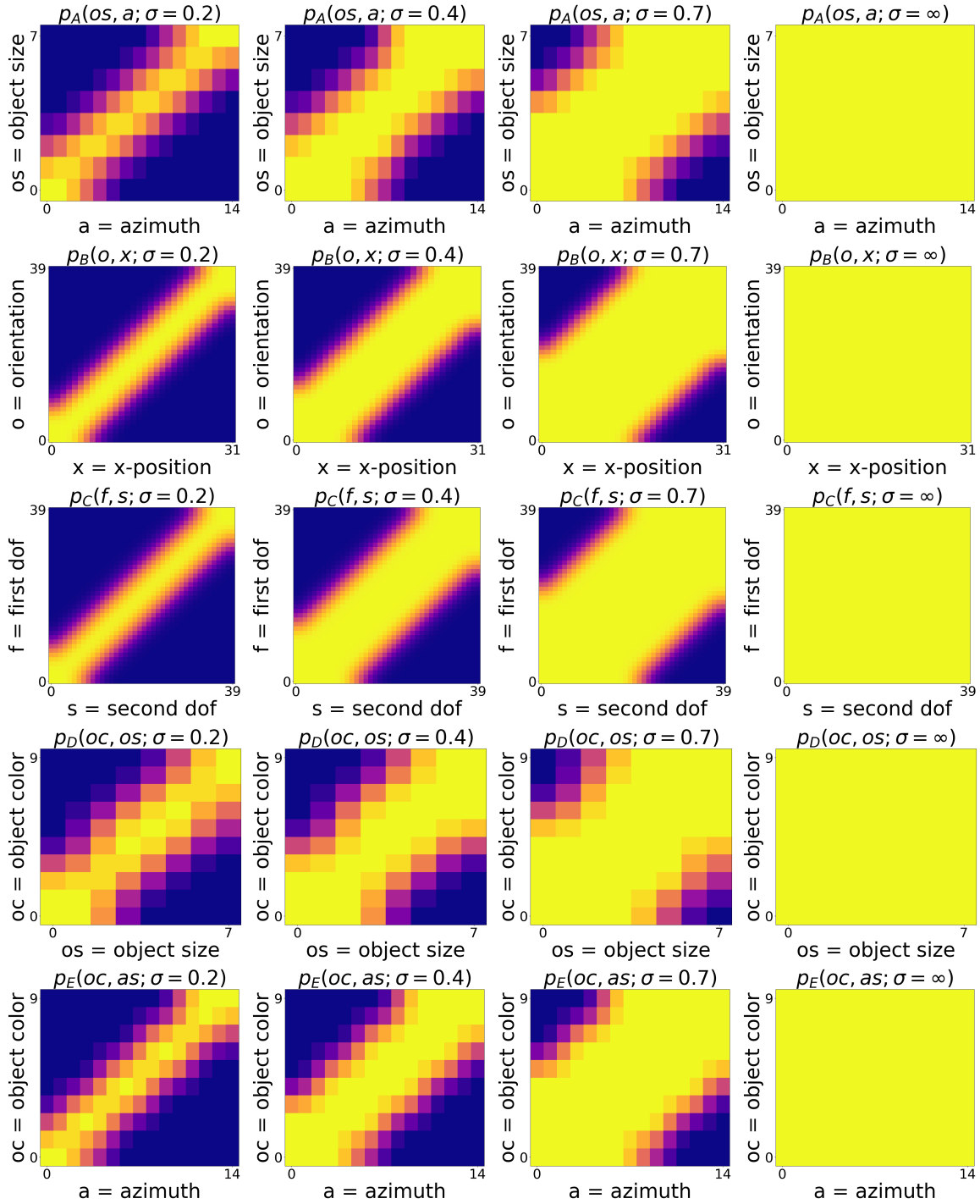


Figure 8: Probability distributions for sampling training data in the correlated pair of FoVs in the respective datasets (A, B, C, D, E) considering correlation strengths of $\sigma = 0.2$, $\sigma = 0.4$, $\sigma = 0.7$ and $\sigma = \infty$, the uncorrelated limit (from left to right).

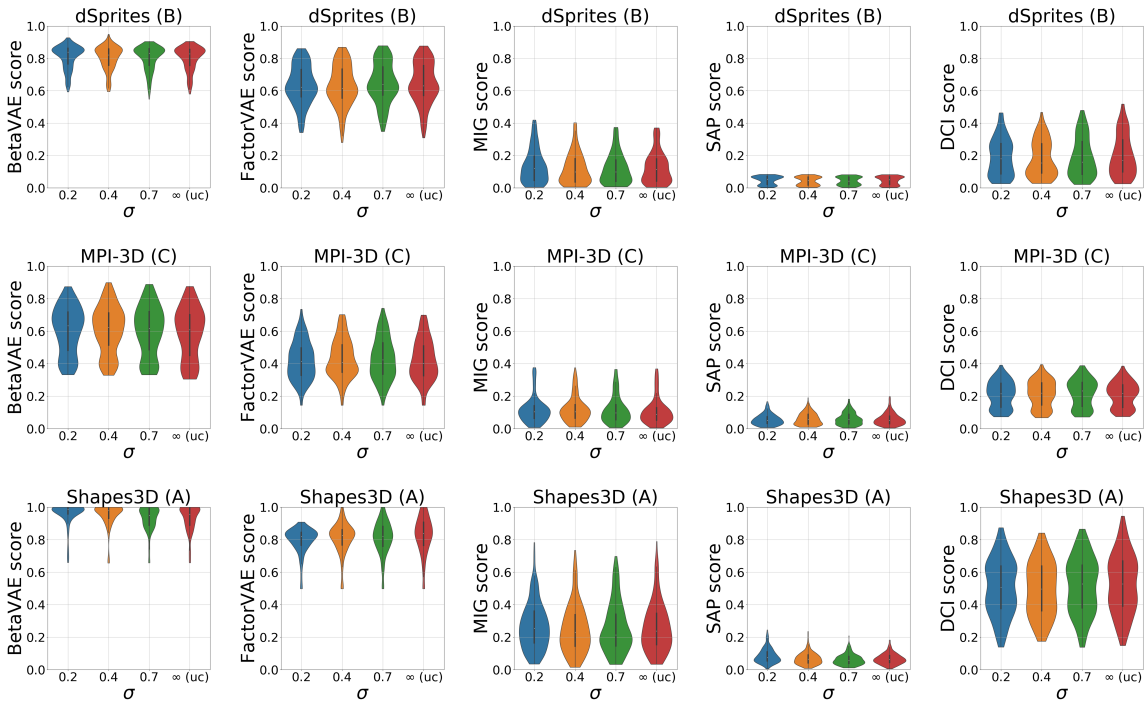


Figure 9: Standard disentanglement metrics evaluated on the correlated training set showing no clear trend for different correlation strengths.

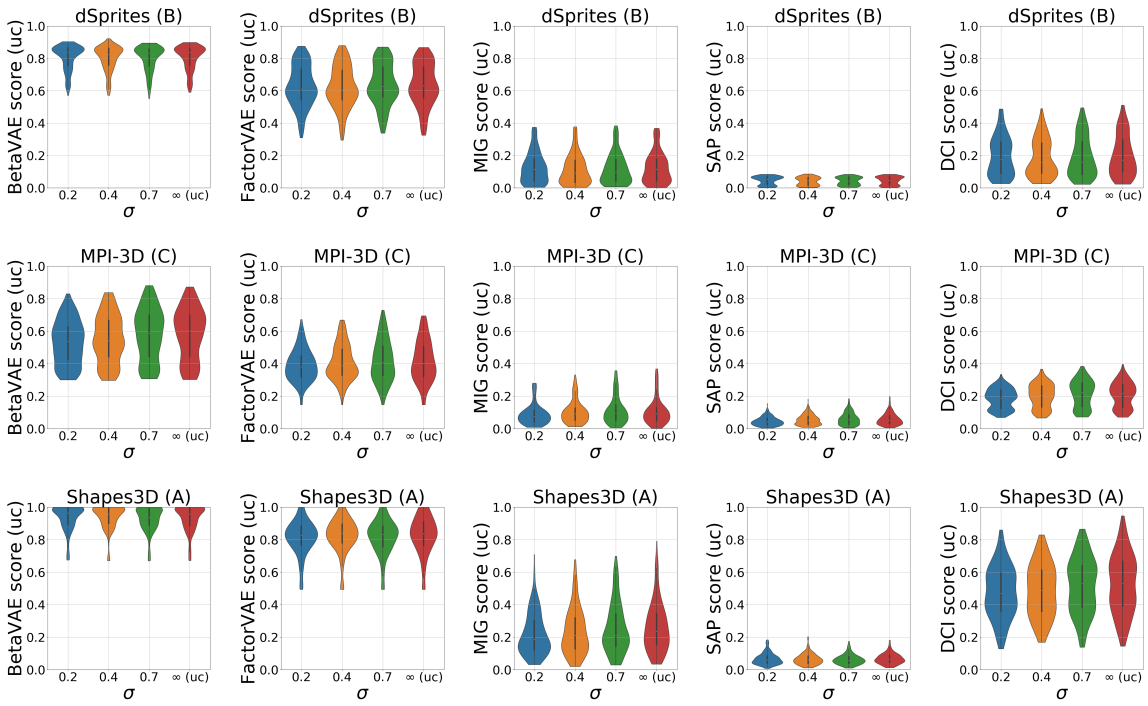


Figure 10: Standard disentanglement metrics evaluated on the uncorrelated training set showing no clear trend for different correlation strengths.

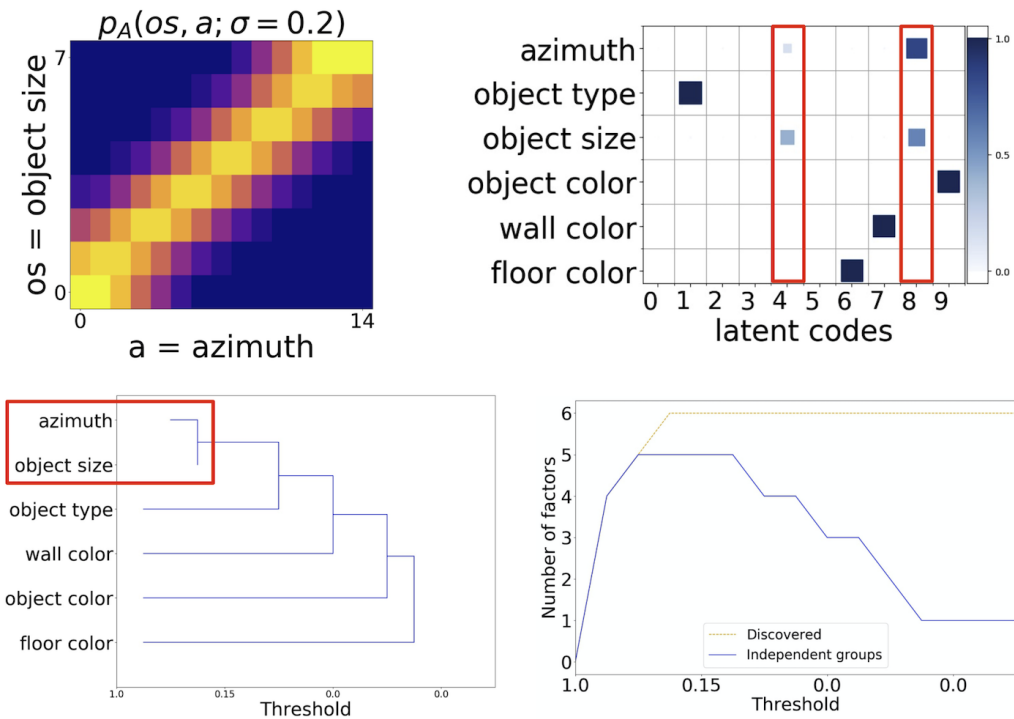


Figure 11: Joint probability distribution with strongest correlation ($\sigma = 0.2$) on Shapes3D (A) (top left). The traversals in latent code no 4 and 8 (highlighted in black), suggest that these dimension encode a mixture of azimuth and object size, reflecting one major axis along the correlation line of the joint distribution (middle) and one smaller, locally orthogonal axis. Shown is an analysis of the best DCO score model among all 1980 trained models on this dataset. The GBT feature importance matrix of this model (top right) indicates existing entanglement of azimuth and object size encoded in latent codes no 4 and no 8. Additional entanglement analysis base on a pairwise threshold metric introduced in (Locatello et al., 2019b) can be seen in the bottom row showing that this pairwise entanglement is too strong to be separated into two independent groups.

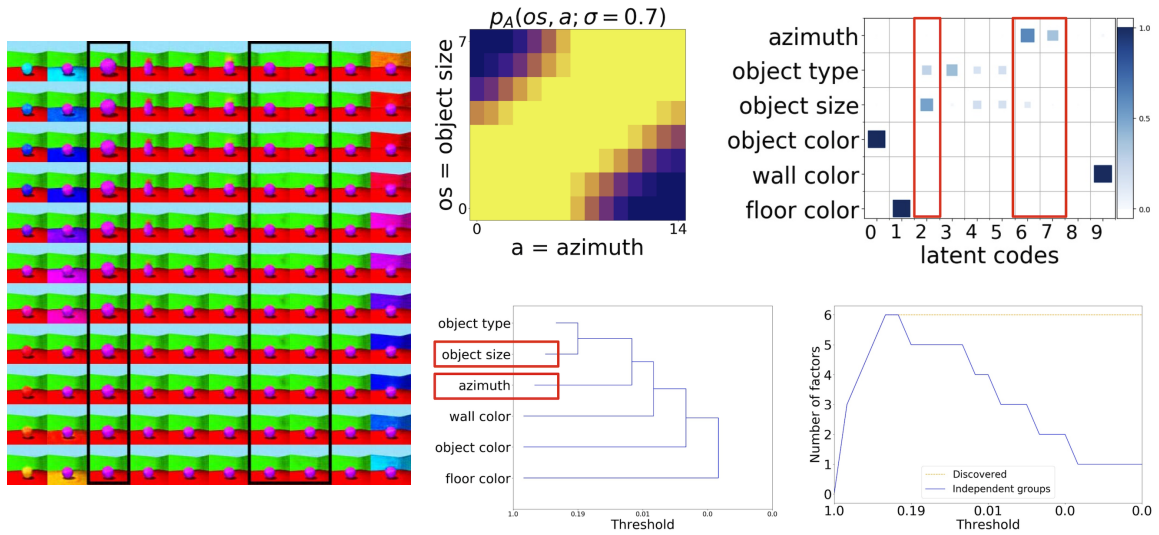


Figure 12: We show latent traversals (left) of the best DCI score model among all 180 trained models with weak correlation ($\sigma = 0.7$) in object size and azimuth. The traversals in latent code no 3 and 7/8 (highlighted in black), suggest that these dimensions encode no mixture of azimuth and object size compared to the models with stronger correlation. This is supported by the GBT feature importance matrix of this model (top right). This pairwise entanglement is small enough to be separated into two independent groups as supported by the dendrogram in the lower part.

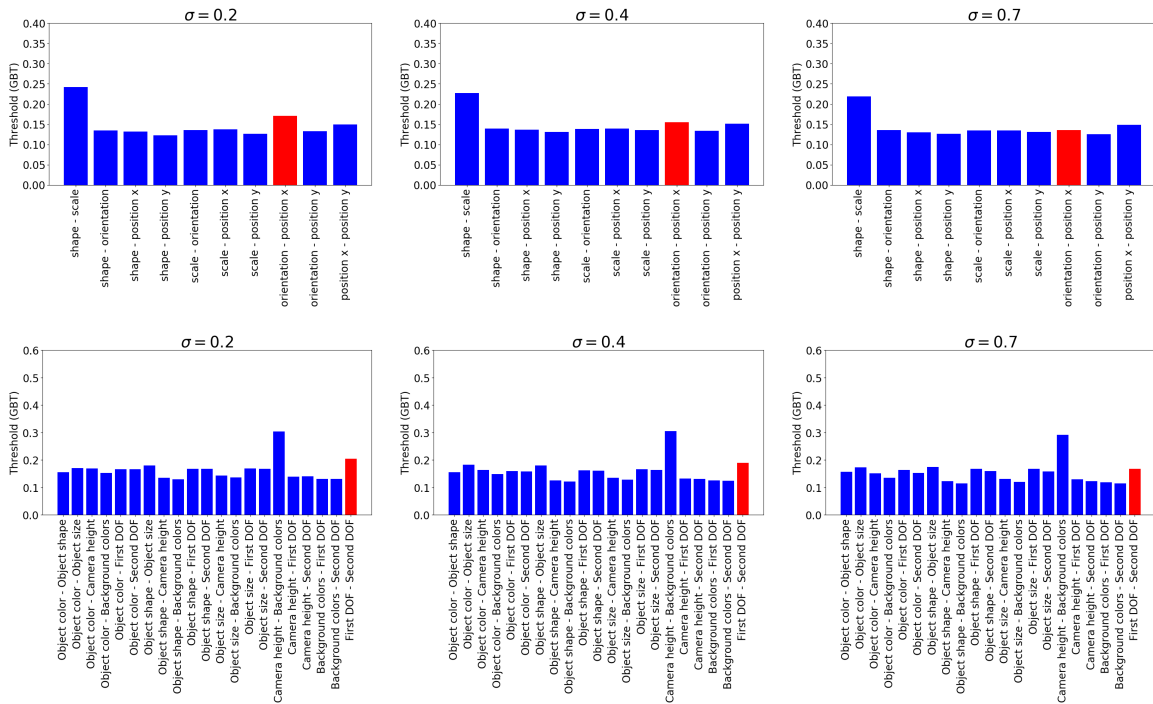


Figure 13: Pairwise disentanglement scores help to uncover still existent correlations in the latent representation. Mean of the pairwise entanglement scores (based on GBT feature importance) across each 180 models in dSprites (B) (upper row) and MPI-3D (C) (lower row), showing that stronger correlation leads to more entanglement. The correlated pair of factors is highlighted (red). The left column corresponds to models trained under a correlation strength $\sigma = 0.2$, the middle column with $\sigma = 0.4$ and the right column with $\sigma = 0.7$.

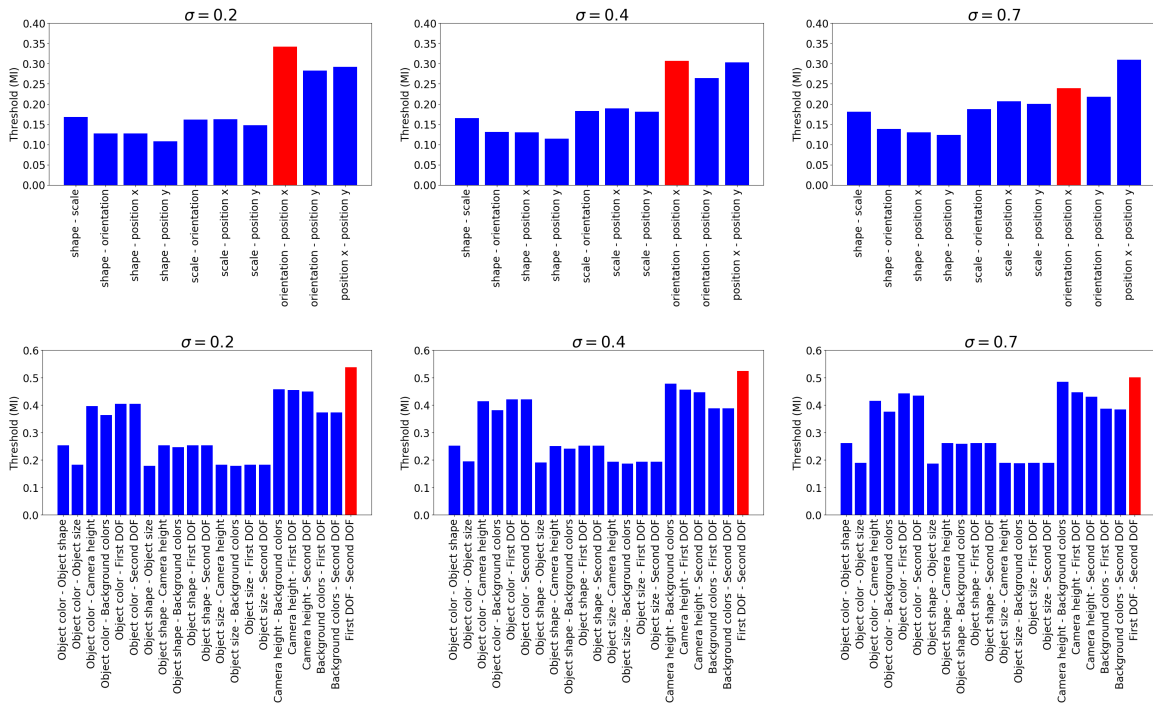


Figure 14: Pairwise disentanglement scores help to uncover still existent correlations in the latent representation. Mean of the pairwise entanglement scores (based on mutual information) across each 180 models in dSprites (B) (upper row) and MPI-3D (C) (lower row), showing that stronger correlation leads to more entanglement. The correlated pair of factors is highlighted (red). The left column corresponds to models trained under a correlation strength of $\sigma = 0.2$, the middle column of 0.4 and the right column of 0.7 .

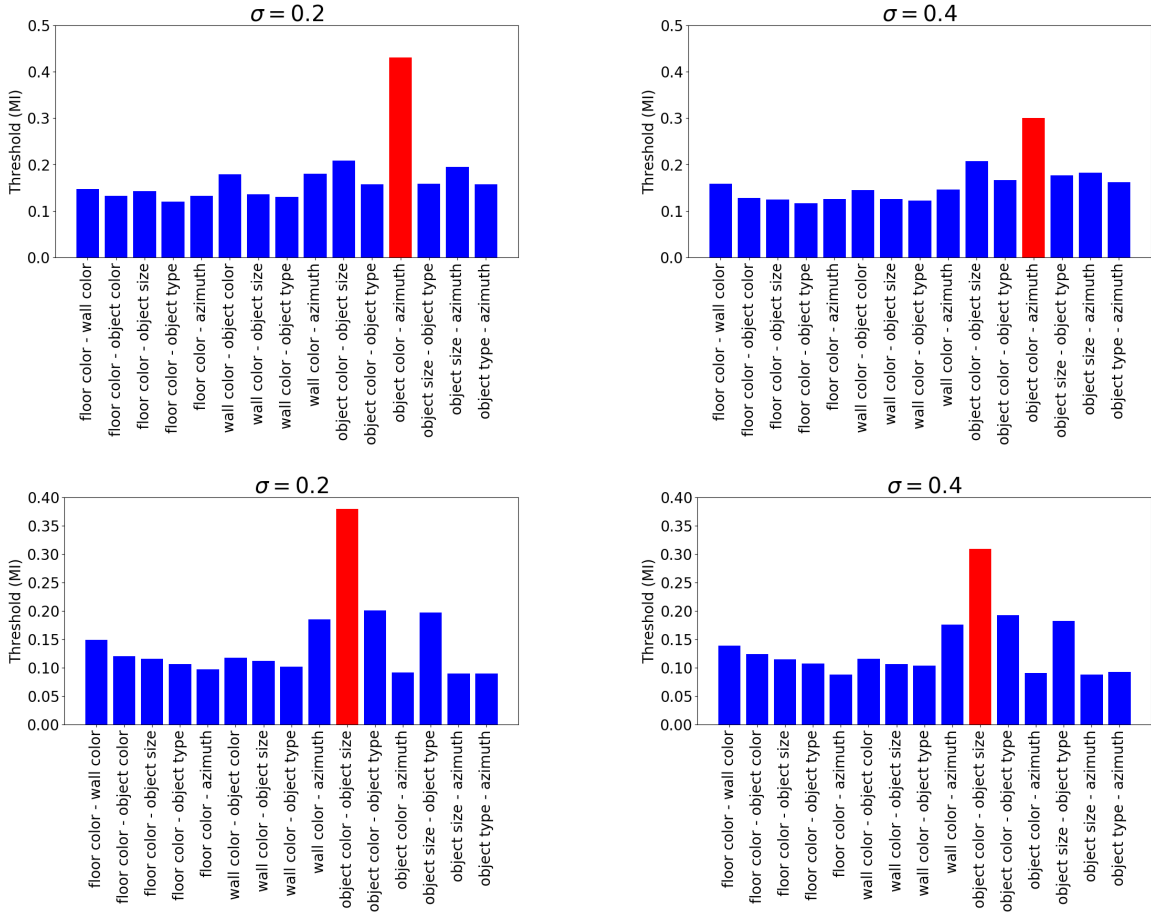


Figure 15: Pairwise disentanglement scores help to uncover still existent correlations in the latent representation. Mean of the pairwise entanglement scores (based on mutual information) across each 180 models in Shapes3D (D) (top row) and Shapes3D (E) (bottom row), showing that stronger correlation leads to more entanglement. The correlated pair of factors is highlighted (red). The left column corresponds to models trained under a correlation strength $\sigma = 0.2$ and the right column with $\sigma = 0.4$.

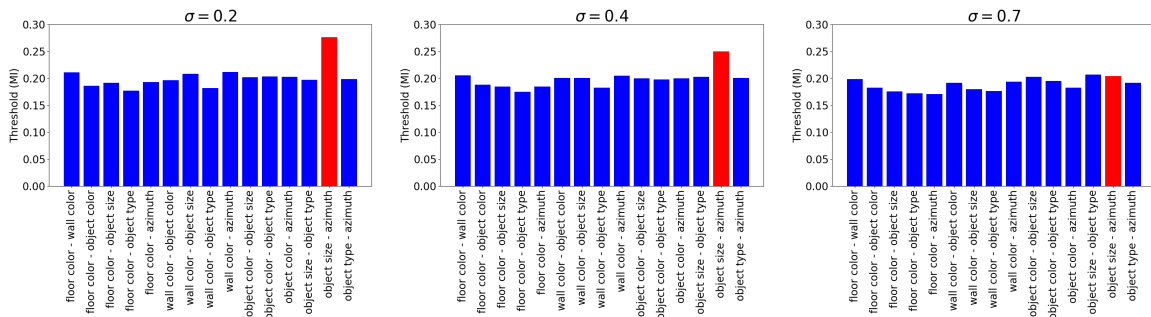


Figure 16: Pairwise disentanglement scores help to uncover still existent correlations in the latent representation. Mean of the pairwise entanglement scores (based on mutual information) across each 180 models in Shapes3D (A), showing that stronger correlation leads to more entanglement. The correlated pair of factors is highlighted (red). The left column corresponds to models trained under a correlation strength $\sigma = 0.2$, the middle column with $\sigma = 0.4$ and the right column with $\sigma = 0.7$. The correlated pair of factors is highlighted in red.

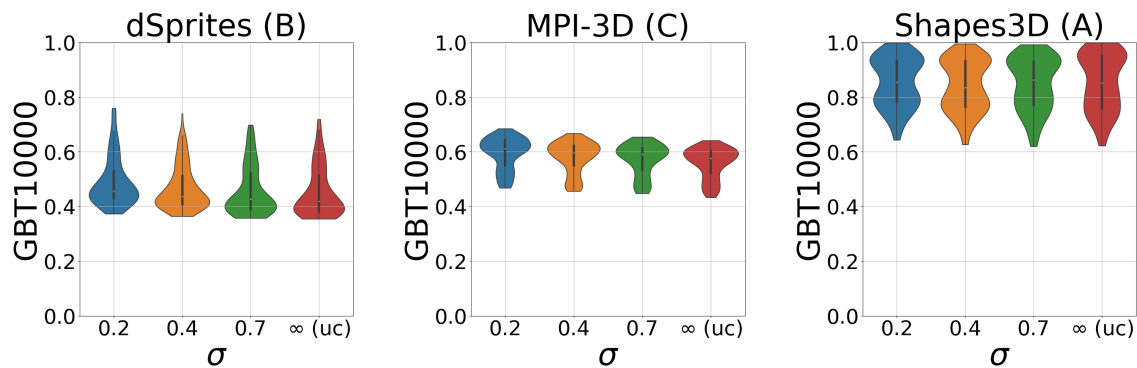


Figure 17: Downstream performance in terms of a GBT classifier to predict the factor of variation from the latent representation.

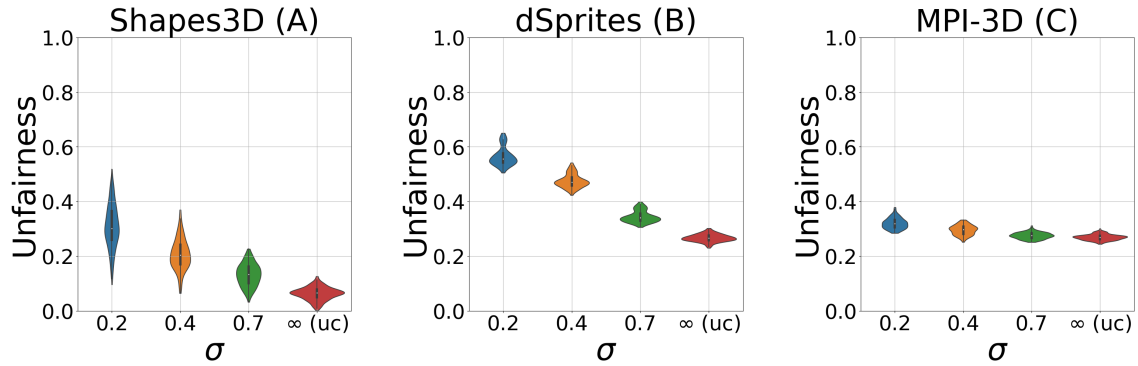


Figure 18: Disentangled representations trained on correlated data are anti-correlated with higher fairness properties. The plots show the mean unfairness scores between the correlated factors with decreasing correlation strength for Shapes3D (A), dSprites (B) and MPI3D-real (C).

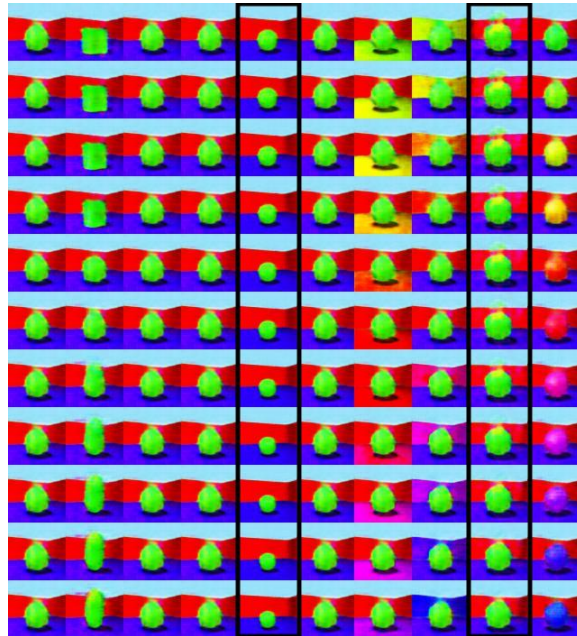


Figure 19: Generalization capabilities towards out-of-distribution test data. Latent traversals from an observations the model has never seen during training. The starting point corresponds to a factor configuration in point 1 from figure 4. Shown are the results of the model with highest DCI score among all 180 trained models on Shapes3d (A) with a very restricted correlation strength $\sigma = 0.2$ in object size and azimuth

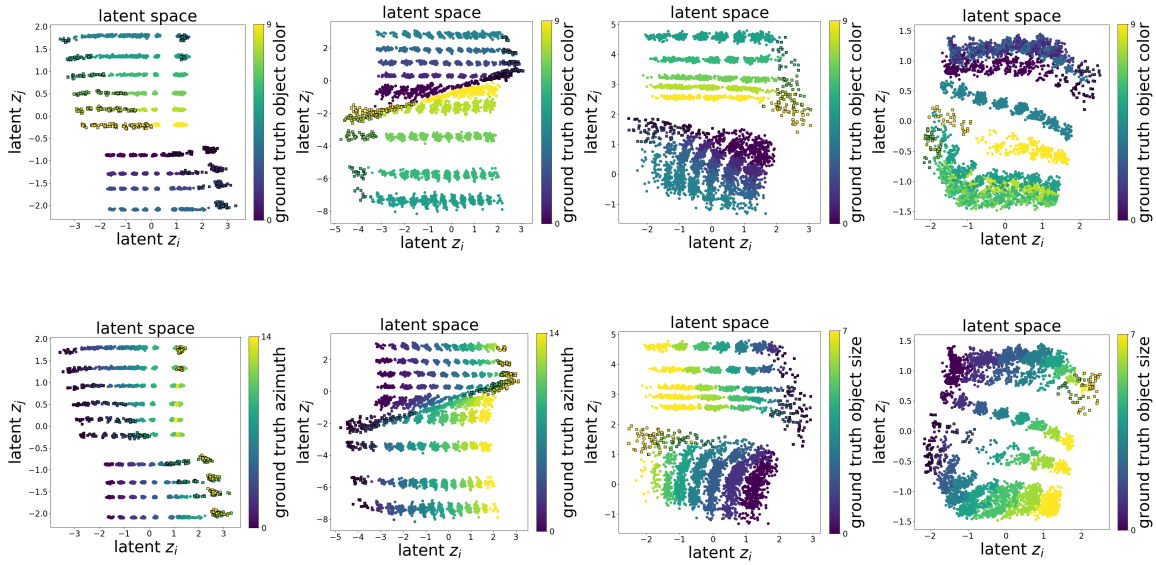


Figure 20: Latent space distribution of the two entangled dimensions of the best DCI model in Shapes3d (E) with $\sigma = 0.2$ (first column), in Shapes3d (E) with $\sigma = 0.4$ (second column), in Shapes3d (D) with $\sigma = 0.2$ (third column) and in Shapes3d (D) with $\sigma = 0.4$ (fourth column). Latent codes sampled from correlated observations (circle without edge) and (2) latent codes sampled with an object size-azimuth configuration not encountered during training (squares with black edge). Each column shows the ground truth values of the two correlated factors by color.

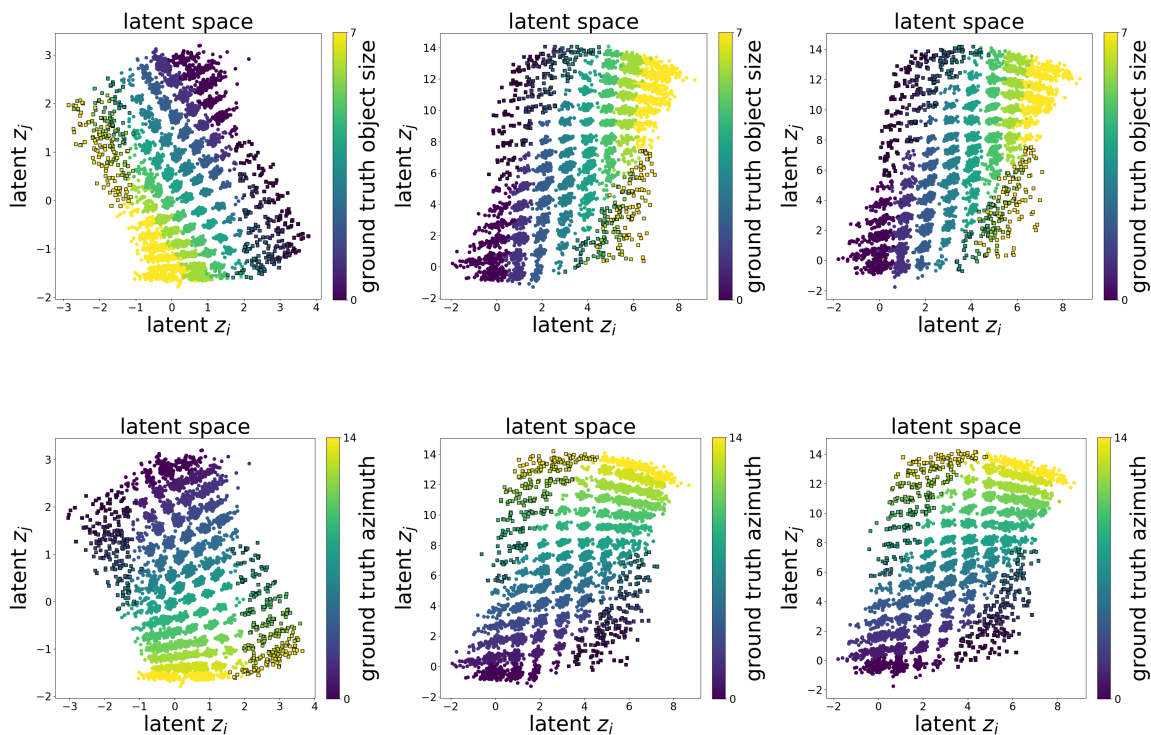


Figure 21: Latent space distribution of the two entangled dimensions of the best DCI model in Shapes3d (A). Latent codes sampled from correlated observations (circle without edge) and (2) latent codes sampled with an object size-azimuth configuration not encountered during training (squares with black edge). Left column shows the ground truth values of the two correlated factors by color. Middle and right column show the fast adapted space using linear regression and 100 or 1000 labels respectively.

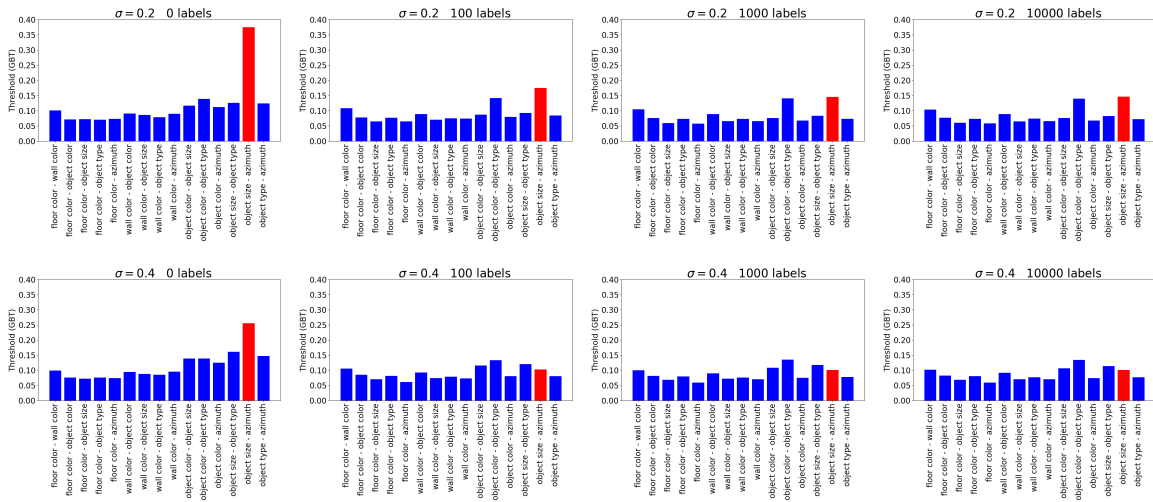


Figure 22: Pairwise disentanglement scores (based on GBT feature importance) for all pairs of variables in Shapes3D (A) with correlation strength $\sigma = 0.2$ (top row) and $\sigma = 0.4$ (lower row). The correlated pairs highlighted (red). Left plot is the unsupervised baseline without any fast adaptation. Other plots show that fast adaption using linear regression reduces these correlations with as little as 100 labels.

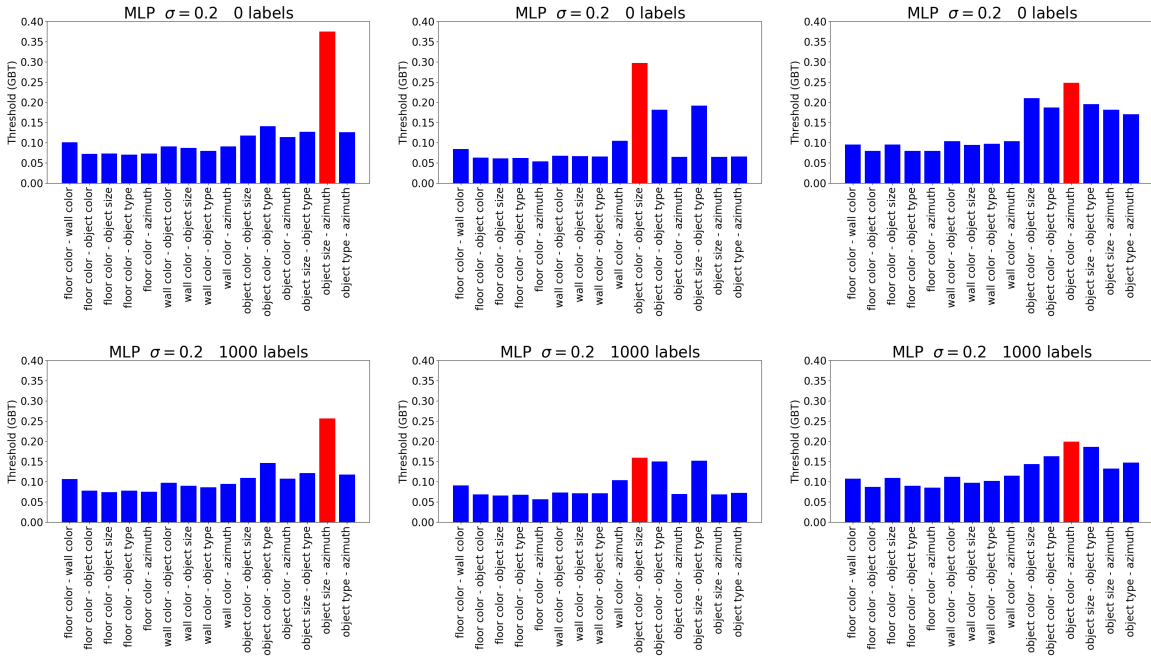


Figure 23: Pairwise disentanglement scores (based on GBT feature importance) for all pairs of variables in Shapes3D (A) (top left), Shapes3D (D) (top middle) and Shapes3D (E) (top right) all with correlation strength $\sigma = 0.2$. The correlated pairs highlighted (red). Top row is the unsupervised baseline without any fast adaptation. Bottom row shows that fast adaptation using a one-hidden layer MLP reduces these correlations with as little as 1000 labels when sampled from the uncorrelated dataset.

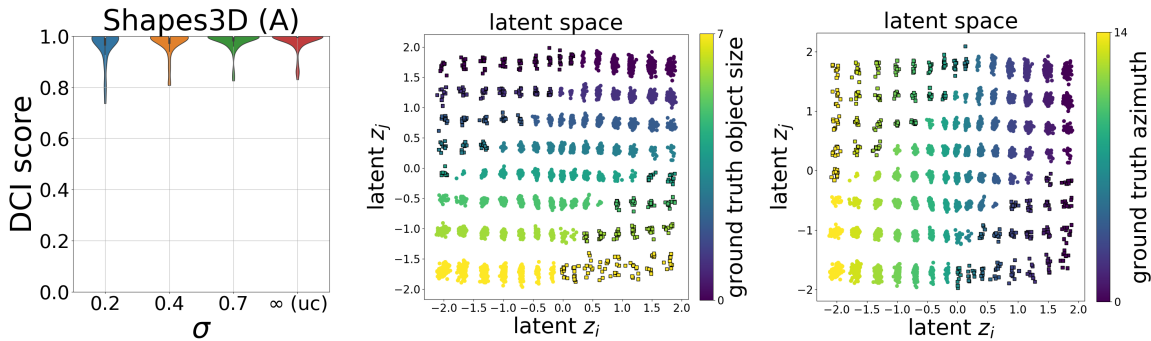


Figure 24: Left: With weak supervision trained models on Shapes3D (A) correlating object size and azimuth learn consistently improved, often perfect, disentangled representation across all correlation strengths. Right: Latent dimensions of a best DCI model with strong correlation (0.2). Representations are perfectly axis-aligned with respect to both of the correlated variables ground truth values (right).

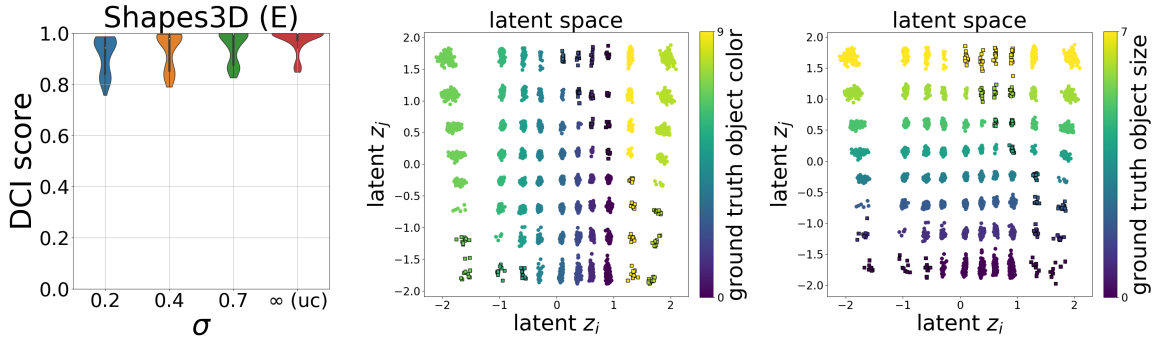


Figure 25: Left: With weak supervision trained models on Shapes3D (E) correlating object color and azimuth learn consistently improved, often perfect, disentangled representation across all correlation strengths. Right: Latent dimensions of a best DCI model with strong correlation (0.2). Representations are perfectly axis-aligned with respect to both of the correlated variables ground truth values (right).

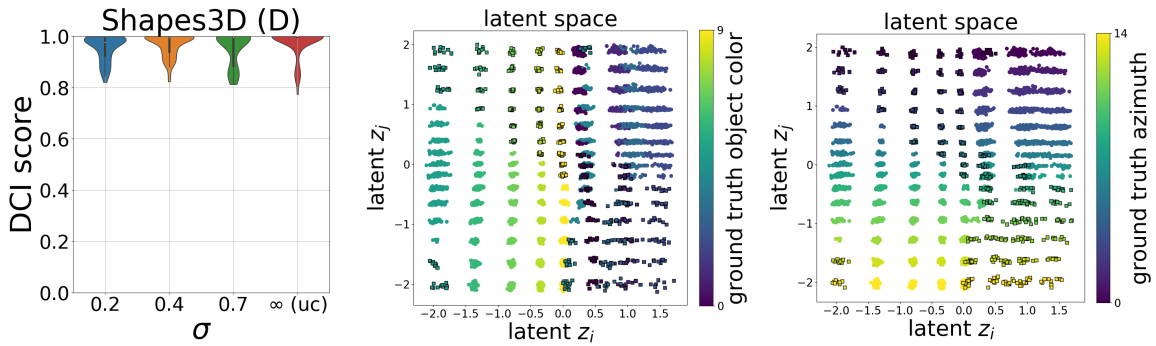


Figure 26: Left: With weak supervision trained models on Shapes3D (F) correlating object color and azimuth learn consistently improved, often perfect, disentangled representation across all correlation strengths. Right: Latent dimensions of a best DCI model with strong correlation (0.2). Representations are perfectly axis-aligned with respect to both of the correlated variables ground truth values (right).

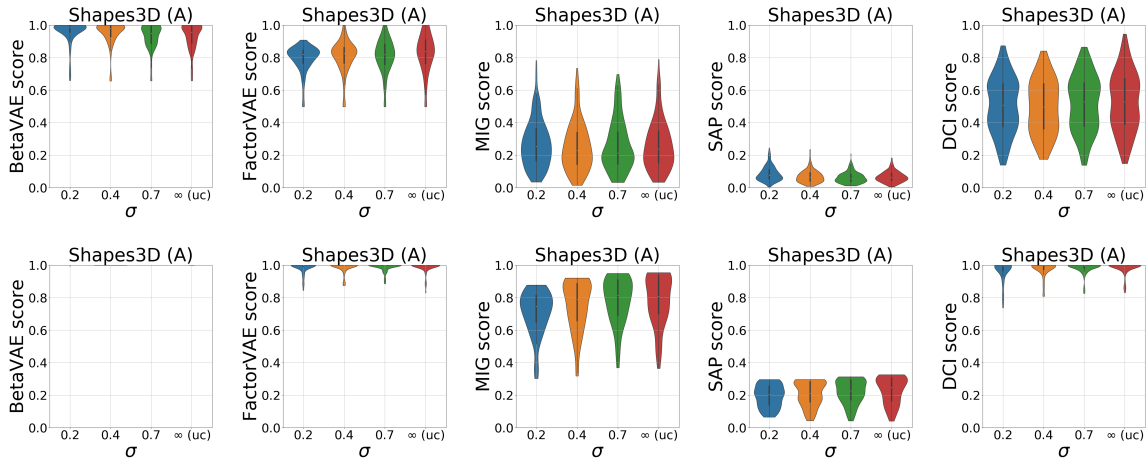


Figure 27: Standard disentanglement metrics evaluated on the correlated training set Shapes3D (A) in the unsupervised (top row) and weakly supervised setting (bottom row).

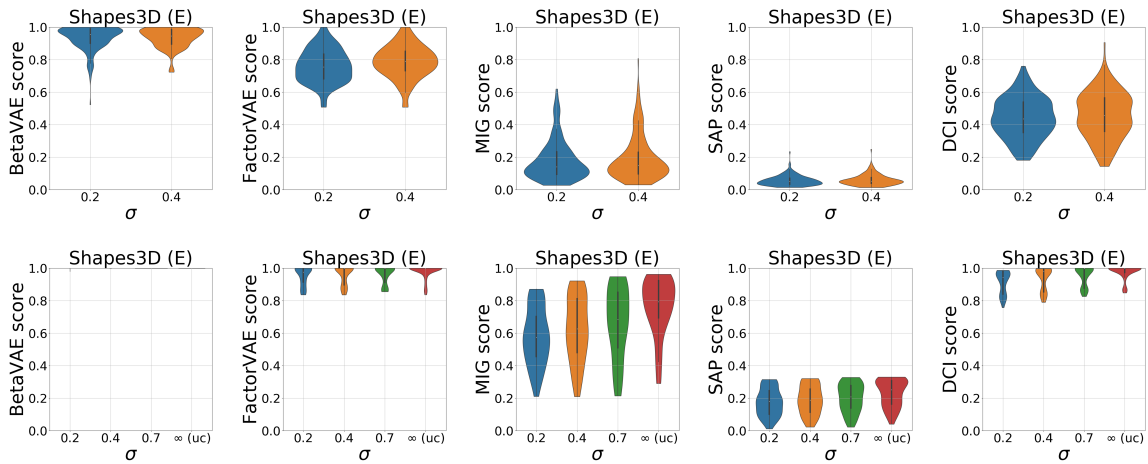


Figure 28: Standard disentanglement metrics evaluated on the correlated training set Shapes3D (E) in the unsupervised (top row) and weakly supervised setting (bottom row).

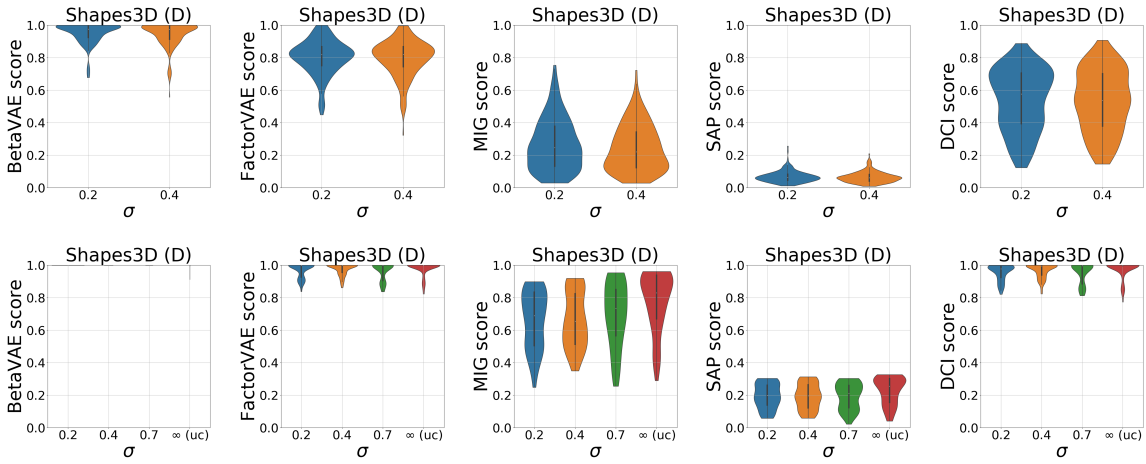


Figure 29: Standard disentanglement metrics evaluated on the correlated training set Shapes3D (D) in the unsupervised (top row) and weakly supervised setting (bottom row)

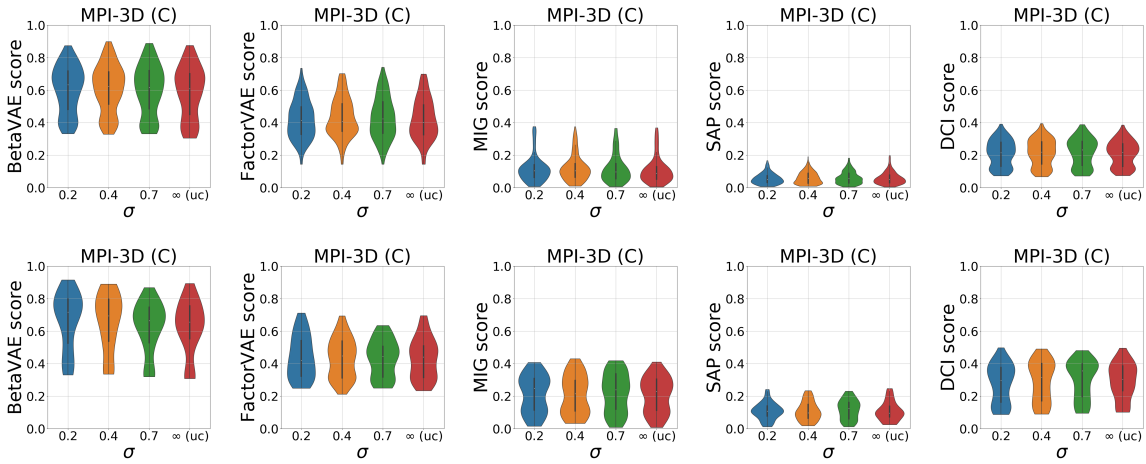


Figure 30: Standard disentanglement metrics evaluated on the correlated training set MPI-3D (C) in the unsupervised (top row) and weakly supervised setting (bottom row).

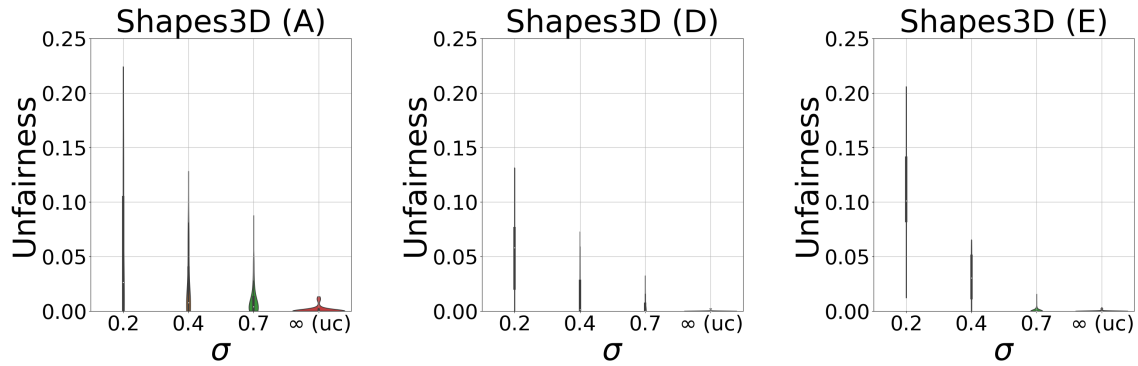


Figure 31: Unfairness between factors that are correlated in training data can be reduced substantially - even for strongest correlations - using the weak supervision method. Shown are the unfairness scores for the three different Shapes3D variants evaluated on the correlated training dataset obtained under weakly supervised training.

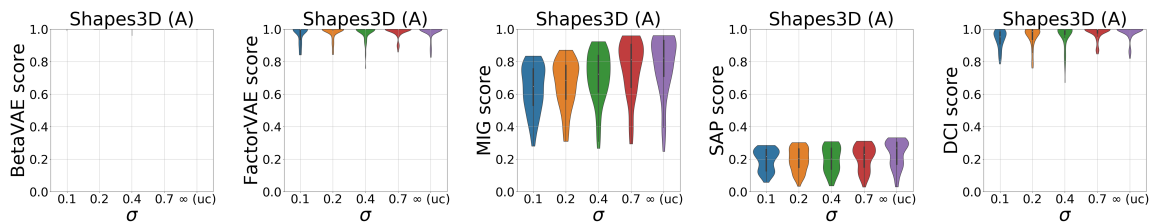


Figure 32: Disentanglement metrics for a given correlation strength across all models when allowing for observation consistent with the causal generative model only.

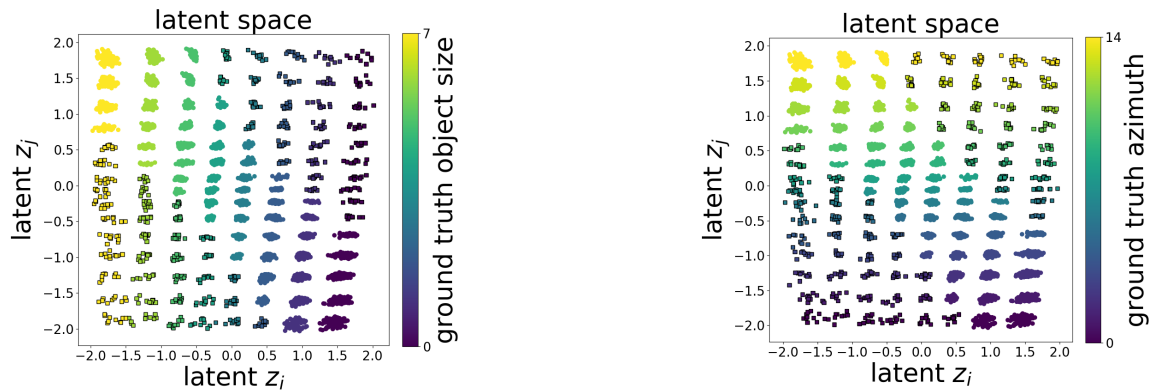


Figure 33: Correlations in training data can be fully disentangled using weak supervision - even under the stronger assumption that sampling of observation pairs follow its causal generative model. Learnt latent space encoding the two correlated factors of variation for a model with $\sigma = 0.1$ and low reconstruction loss.